VOL. 17, NO. 4, FEBRUARY 2022 ISSN 1819-6608
ARPN Journal of Engineering and Applied Sciences

www.arpnjournals.com

NUMERICAL STUDY ON CRASHWORTHINESS OF POLYGONAL CROSS-SECTION THIN-WALLED BEAMS UNDER QUASI STATIC BENDING

Sanjay Patil, Arvind Bhosale, Vijaypatil Dhepe, Dheeraj Lengare, Kiran Bansode and Rashtrapal Teltumade
Department of Automobile Engineering, Government College of Engineering and Research, Avasari (kh), Pune, Maharashtra, India
E-Mail: sdpatil.auto@gcoeara.ac.in

ABSTRACT

Higher energy absorption efficiency and better crashworthiness performance are always the primary goals of researchers. This paper aims to study the bending collapse bahaviour of polygonal cross-sectional thin wall beam (TWB) under quasi statics bending. TWB are commonly used as energy absorbers in automobiles due to their light weight and high energy absorption capacity. TWB that is circular or square is frequently used inside vehicle doors. This beam deforms and absorbs the maximum impact energy in the event of a side collision than other components of doors. The crashworthiness of polygonal cross-section TWBs subjected to bending load was investigated using numerical simulations, and they were compared to the corresponding circular and square cross-section TWBs. In this work polygonal TWB ranging from the pentagon to the dodecagon are considered for analysis. To evaluate the bending collapse performance of beams, specific energy absorption and crash force efficiency crashworthiness indicators are used. Finite element simulations were conducted in ABAQUS explicit dynamic software, and all polygon plastic hinges and flattening patterns were examined. The results show that heptagon, octagon, and nonagon cross-section TWB outdo square and circular TWB in crashworthiness performance.

Keywords: energy absorption elements; specific energy absorption; crash force efficiency; flattening patterns, plastic hinges.

INTRODUCTION

There has been a lot of activity in the past few decades on crashworthiness of thin-walled beam. Thin-walled beams (TWBs) are commonly applied for crashworthiness applications because of its advantages in terms of light weight, high strength and stiffness, low cost as well as superior energy absorption capacity [1]. They are commonly employed in automobiles, special-purpose vehicles, roll-over and falling object protective structures, and other areas subject to crash safety requirements [2]. The beam deforms and absorbs a large amount of energy at the time of impact [3]. Many different cross-sections of TWB's are available such as round, rectangular, square, and elliptical [4].

TWBs with varying cross sections, thicknesses, diameters, materials, etc. are compared by Crashworthiness indicator like Energy Absorption (EA), Specific Energy Absorption (SEA), average crash force (F_{avg}) and Crash Force Efficiency (CFE) are crashworthiness indicators [4,5].

EA indicator is measured the total energy absorbing capacity of a TWB and it is evaluated by calculating the area under the force displacement curve of the bending process. A higher EA value implies that the beam has a greater ability to absorb energy during the bending. A mathematical for EA is,

$$EA = \int_0^d F(x).dx \quad (1)$$

Where F(x) is the crash force, d is the deformation of beam.

The SEA indicator measures the amount of energy absorbed per unit mass of the beam, and thus, it reflects the structure's efficiency. A mathematical equation for SEA is,

$$SEA = \frac{EA}{Massofbeam} \quad (2)$$

F_{avg} is the average value of crash force during the whole bending process, and F_{max} is the maximum force during the bending process. The ratio of average force to maximum force is called Crash Force Efficiency, which indicates the steadily of bending process . Thus,

$$CFE = \frac{F_{avg}}{F_{max}} \quad (3)$$

The collapse behaviour of TWBs under bending can be understood using a various theories. The flattening pattern associated with the bending deformation of a cylinder was initially identified by Brazier. The cross section of a beam flattens as the deformation progresses when it is subjected to bending. As the cross section flattens, the bending stiffness of the beam decreases, and beam deforms largely as a result of the imposed crush force [6, 7]. Flattening patterns are studied experimentally and theoretically by many researchers, including W. Abramowicz [8], Hamidreza Saadatfard [10]. Second popular theory was given by Kecman [9], according to analytical and experimental research on square and rectangular tubes, when a thin wall beam is subjected to a bending load, the cross section starts to deform plastically. These plastic deformations occur over some folding lines, which are called "hinge lines". The progression of plastic hinge movement drives the crashworthiness performance of the circular beam. Many researchers have used this hinge line model and found good agreement between

numerical and experimental results, including M. Elchalakani *el al*. [11], S. Poonaya's *el al*. [14], Hakim S *el al.* [25] etc. Recently, many researchers are using the Koteko [12] yield line mechanism (YLM) model, when TWB fails due to bending, the cross-section walls undergo plastic folding and collapse in a spatial plastic mechanism. YLM analysis of the collapse mechanism provides a bending moment-rotation relationship as in Eq.4, from which energy absorption capacity of the TWB can be estimated,

$$M(\theta) = \frac{dW}{d\theta} \quad (4)$$

Where, W is the total energy absorbed by yield line, θ is the rotation angle of TWB, the total energy absorbed can be evaluated by,

$$W(\theta) = \sum_i^n W(\theta) \quad (5)$$

Where, 'W' is the energy absorbed by each yield line and 'n' is the number of yield lines in the model. Soheila Madulia *et al.* [13] examined steel hollow sections using YLM model and found that YLM collapse curves are in good agreement with the real experiment graphs.

To determine and increase the energy absorption capability of these structures, substantial numerical and experimental research has been undertaken. The beam thickness, material, loading angle, and cross section of a TWB effects on its crashworthiness, the impact of beam thickness on crashworthiness is the greatest of them. [16, 18, 19]. Hamidreza Saadatfard *el al*. [10] from experimental and numerical results illustrate that by increasing the wall thickness, the EA of the beam increases. To increase the crashworthiness of the TWB, Haksung Lee *el al.* [15] used Glass Fiber Reinforced beams. Whereas, Guangyong Sun *et al*. [17] employ a functionally graded thickness tube (FGT). The FGT tube absorbs more energy than the uniform thickness tube. Zonghua Zhang [20] and Ali Ghadianlou *et al*. [21] used various rib arrangements. Some researchers investigated various cross section beams in order to compare their crashworthiness. According to [22, 24], the rectangular cross section has a higher CFE than the square section, but the square section has a higher SAE than the rectangular cross-section beam. Muhammed Emin Erdin *el al*. [26] studied quasi static axial crushing mechanism of FGT, universal testing machine were used to apply the quasi-static axial compression load. In order compared the performance of FGT SEA and CFE indictors were used. Chen *et al*. [27] investigated the flattening ratio and found that tube thickness and material properties influence the flattening pattern during plastic bending. Patil *et al.* [28] perfumed the numerical simulation on polygonal cross section beam at lateral impact.

Considering recent investigation in details, less exposure has been seen in the crashworthiness of polygonal cross-section TWBs in the literature. The bending collapse behaviours and crashworthiness of different polygonal cross sections of TWBs under quasi statics are explored in this article using numerical analysis, and the flattening and bending patterns of beams are analyzed. The weight and thickness characteristics of the TWB are kept the same for all TWBs as it influences crashworthiness. Polygonal cross-section TWBs are compared to circular and square cross-section TWBs in terms of crashworthiness. ABAQUS explicit dynamic software was used to perform the numerical simulations. Experimental results from the literature were used to validate the numerical simulation setup.

MATERIALS AND METHODS

To analyze the crashworthiness of various polygons, a quasi-static type explicit dynamic simulation has been performed, and crashworthiness indicators are used to evaluate the beam's performance.

Material and Geometry of Polygon

All polygonal profiles are 2mm thick, and the weight of each polygon is kept constant at 0.130kg by altering the polygon's edge length. Table-1 shows the dimensions of all polygons. Where 'O' denotes the polygon's outer radius.

Table-1. Dimension of polygon.

Profile No.	Name of polygon	O (mm)	Geometry
POLY 4	Square	26 (edge length)	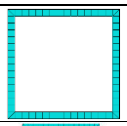
POLY 5	Pentagon	21.2	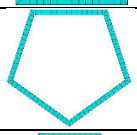
POLY 6	Hexagon	19.5	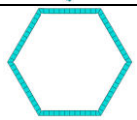
POLY 7	Heptagon	18.5	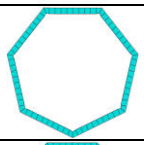
POLY 8	Octagon	17.9	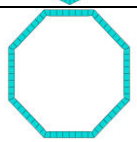
POLY 9	Nonagon	17.6	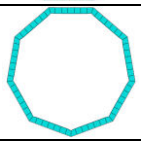
POLY 10	Decagon	17.3	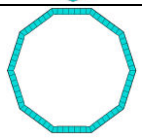
POLY 11	Hendecagon	17.1	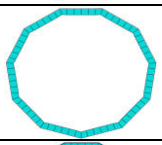
POLY 12	Dodecagon	17	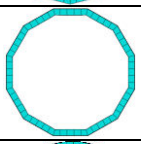
CIR	Circular	16.3	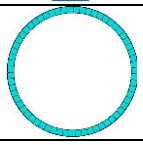

Aluminum alloy AA1100-O has been used to model the polygonal TWB. The stress-strain curve and material properties are adopted from literature [23] and shown in figure Figure-1 and Table-2 respectively.

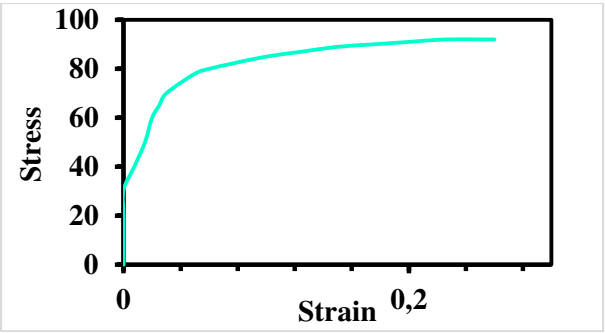

Figure-1. Stress-strain Curve of AA1100-O.

Table-2. Material properties.

Material Properties	Values
Young's modulus (E)	67.5 GPa
Initial yield stress ($\sigma_{y)}$	30 MPa
Ultimate tensile stress ($\sigma_{u)}$	90 MPa
Poisson's ratio (ν)	0.33
Density (ρ)	2.1 kg/m3

Numerical Simulation Setup

In order to analyze the bending performance of TWB, three-point bending test has been performed numerically. The schematic of simulation setup and geometrical parameters are provided in Figure-2 and Table-3, respectively, where 'el' is the edge length of square beam, 't' is the beam thickness, and 'l' is the beam length. A cylindrical support with a diameter of 'r' and a span of supports is 's'. A cylindrical punch with a diameter of 'R' is move circumferentially on the beam with a velocity of 'V' at the mid-span of the beam.

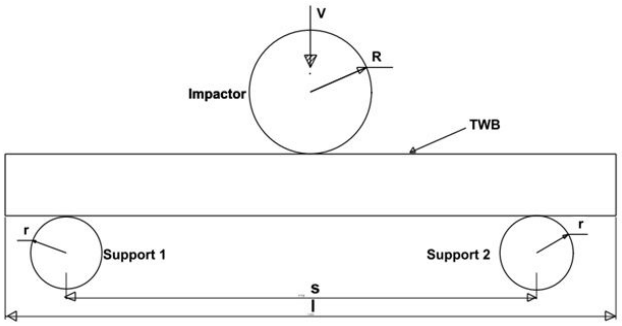

Figure-2. Systematic of simulation setup.

Table-3. Simulation properties.

l(mm)	s(mm)	R (mm)	r (mm)	t(mm)	el
250	200	10	10	2	26

The punch and supports are treated as rigid bodies, whereas the beam is treated as a solid body with a thickness of 2 mm. For the punch, one direction translation displacement is allowable, and for supports all degrees of freedom are fixed. A coefficient of friction of 0.2 is considered at all surface to surface contacts between the punch, beam and supports. In ABAQUS, the 'All with self' surface friction pair is used to avoid interference of surfaces during beam bending. The velocity of the punch is 0.5 m/s and displacement approximate 100mm to obtained information about energy absorption and crash force efficiency. Figure-3 shows the finite element model of the POLY 4 profile. For supports and TWB, four-node shell continuum (S4R) and Hex elements are used, respectively. In order to evaluate the optimum mesh size to balance the computational time and solution accuracy, a convergence test with five different element sizes was carried out on POLY 4 profile. The mesh convergence results are shown in Figure-4. It can be observed that the relative error between element size 2 mm and 3 mm is less than 2% for both EA and F_{avg} parameters.

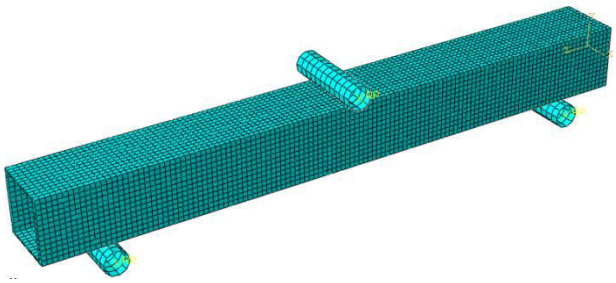

Figure-3. Numerical simulation model.

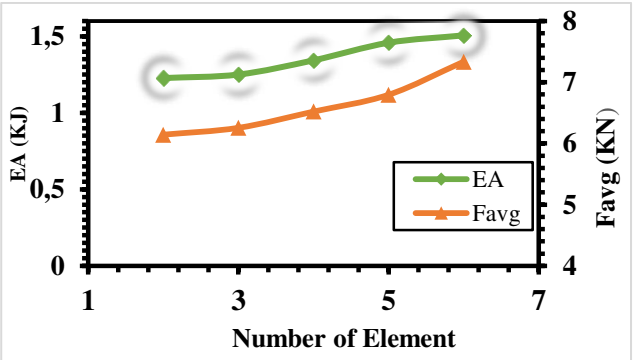

Figure-4. Convergence results of element sizes.

Validation of Simulation Setup

The numerical simulation results are compared with experimental test results published by Xiong Zhang *et al*. [23] before evaluating the crashworthiness indicators of various profiles. Xiong Zhang *et al.* [23] performed a three-point bending test on a square tube with a side length of 26mm and a thickness of 2mm for validation. The tube is made of Aluminum alloy AA1100-O material. The punch velocity is 0.5 m/s, and the displacement is 50 mm. Similar [23] experimental setup parameters are used in this work for the validation. Figure-5 shows the beam deformation from experimental and numerical simulation, while Figure-6 compares the crashworthiness indicators obtained from experimental testing [23] and numerical simulation.

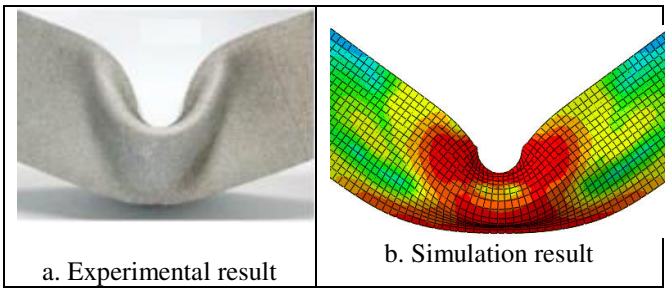

Figure-5. Comparison of beam deformation pattern obtained from experimental [23] and simulation result.

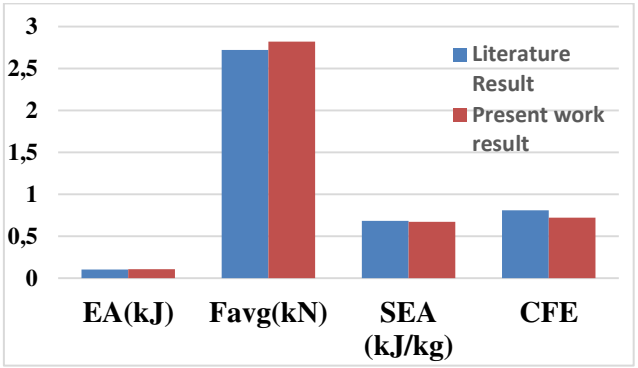

Figure-6. Crashworthiness indicators Numerical v/s experimental result of [22].

The experimental results in the literature [23] are quite similar to the simulation results, with an absolute error of less than 5%, hence this simulation setup is being considered for further investigation.

RESULTS AND DISCUSSIONS

The crashworthiness indicators are evaluated using equations 1, 2, and 3. SEA, CFE of all profiles are discussed in the following subsection.

Maximum Crash Force (F_{max}) and Force–Displacement Characteristics

For convenience of explanation, Figures 7, 8, and 9 shows force displacement diagrams for profiles POLY 4, 5, 6, profiles POLY 7, 8, 9, and profiles POLY 10, 11, 12, CIR, respectively. Figure-10 represents the bending and cross section flattening pattern of all profiles at simulation time frame15.

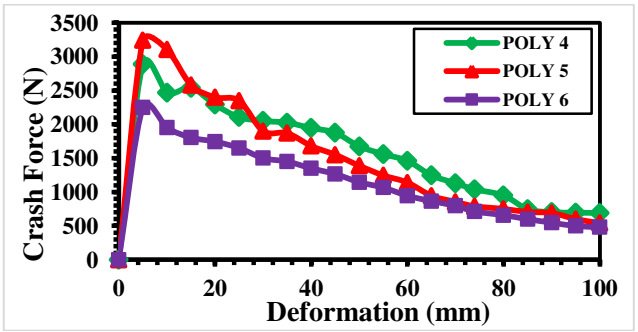

Figure-7. Force- Disp. curve of Profile POLY 4, 5 and 6.

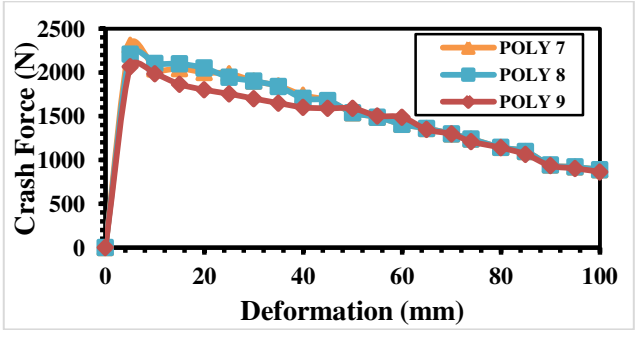

Figure-8. Force- Disp. curve of Profile POLY 7, 8 and 9.

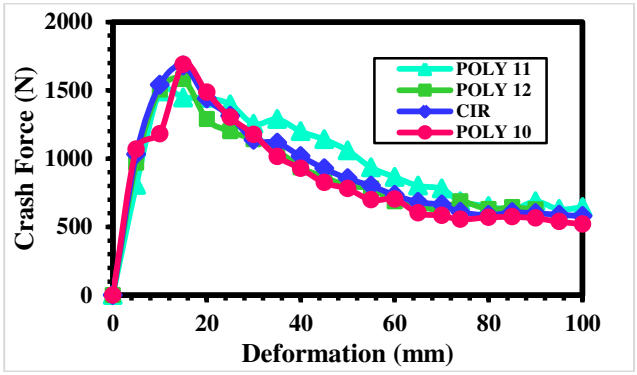

Figure-9. Force- Disp. curve of Profile POLY 10, 11,12 and CIR.

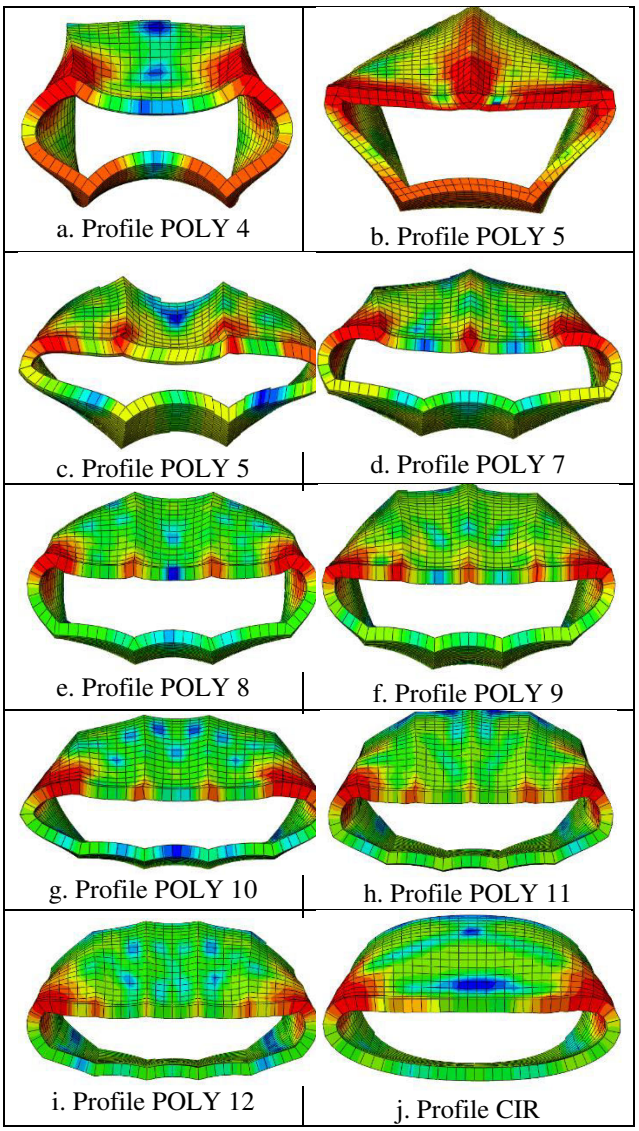

Figure-10. Bending and cross-section flattening pattern of beams at frame 15.

As shown in Figures. 7 and 9, F_{max} is higher for profiles POLY 4, 5, and 6 than for profiles PLOY 11, 12, and CIR. The highest F_{max} of profile POLY 4 is 3.2kN, whereas the lowest F_{max} of profile CIR is 1.6kN. This

implies that the flattening resistance of the profiles in Fig. 7 (POLY 4, 5, 6) is higher than the flattening resistance of the profiles in Figure-9 (POLY 10, 11, 12, CIR) under quasi statics bending.

It is also seen that the F_{max} of profiles shown in Figure-8 (POLY 7, 8, and 9) is in between the profiles in Figure-7 and 9. The crash force achieves an initial peak as a result of the profile's resistance to flattening, when plastic hinges begin to emerge, then the crash force drops due to the folding of profile edges. From flattening patterns shown in Fig. 10, the plastic hinges are starting to form along the edges of profiles POLY 4 and 5, so they can offer greater resistance and absorb more energy during bending, while plastic hinges are starting to form at the corners of polygons for profiles POLY11 and 12, so they can offer less resistance and absorb less energy during bending.

Specific Energy Absorption (SEA)

SEA refers for absorbed energy per unit mass of the beam. Plastic hinges are responsible for the beam's bending capability, as described in the preceding section. So profiles POLY 4, 5 are absorbed more amount of energy comparable profiles CIR, POLY 11 and 12. As a result, POLY 4, 5 profiles have a higher SEA, whereas the CIR, POLY 11 and profiles have a lower SEA. The SEA indicator with a higher value indicates that the structure is more efficient in energy absorption, and therefore POLY 4 and 5 are more efficient. Whereas profiles POLY 9 and 10 have moderate efficiency, and profiles POLY 11, 12, CIR profiles have lower efficiency under quasi statics bending loading.

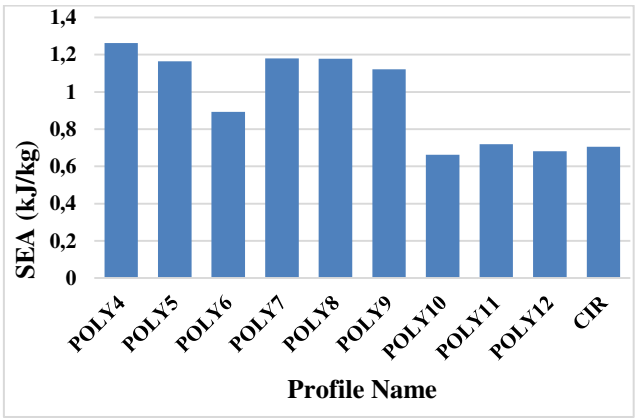

Figure-11. Specific Energy Absorption of beams.

Crash Force Efficiency (CFE)

The bending force should be almost constant throughout the bending operation for consistent deformation. CFE, a dimensionless number, illustrates this. CFE is a number that ranges from 0 to 1. When energy absorption decreases as beam deformation increases, the CFE indicator value tends to zero. Similarly, if the amount of energy absorbed is almost constant during the bending operation, the CFE value is closer to 1. Figure-12 shows the CFE of each profile.

The force-displacement curve shown in Figure-7, for POLY 4, 5 and 6 profiles, the crash force reaches its maximum level, and when plastic hinges are begin to develop on edge or cornel of the polygon, the crash force is considerably reduced. The flattening pattern of these profiles is shown in Fig. 10. Finally, the F_{avg} of the entire bending process is much lower than F_{max}. As a result, the CFE indicator is lower.

The force-displacement curve of profiles POLY 7, 8, and 9 is shown in Figure-8. The crash force is considerably steadier, as can be observed from Figure-8. The plastic hinges progressively create more than one number of edges and corners polygons, as seen in the cross section flattening pattern of these curves in Figure-10, thus the crash force of these profiles is more stable than profiles POLY 4, 5, and 6. Finally, the difference between F_{avg} and F_{max} is lower, and these profiles have a higher CFE than others. The CFE of POLY 9 is 0.70, which is the highest of the profiles. Profile PLOY 10, 11, 12, and CIR have CFE values in the between both cases.

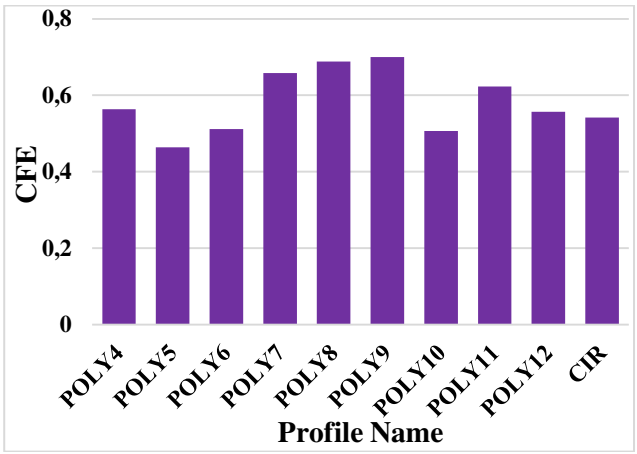

Figure-12. CFE of beams.

CONCLUSIONS

At constant weight and thickness the crashworthiness of a various polygonal cross-section TWB under quasi-static bending was investigated using numerical simulation in this work. Crashworthiness indicators have been substantially influenced by the development of plastic hinges and the cross-section flattening pattern of the beams. The SEA values of the square and pentagon (POLY4and 5) are greater because they have longer edges and so provide stronger deformation resistance. When plastic hinges begin to form, their bending resistance plummets, and the CFE value of these beams drops sharply as well. Due to their shorter edge length, hendecagon and dodecagon (POLY 11and 12) profile beams have lower bending resistance. These beams have a plastic hinge pattern that resembles as circular cross section beam. Plastic hinges developed on edges and corners of heptagon, octagon, and nonagon profile cross-section beams. As a result, they give greater deformation resistance. Higher SEA and CFE values make them more acceptable for crashworthiness.

In this work constant edge thickness polygon has been used, the research may be expanded using varying edge thickness polygon. Similarly, crashworthiness performance of various polygon can be studied under axial loading.

REFERENCES

[1] Javier Luzon-Narroa, Carlos Arregui-Dalmasesb, Luis M. Hernando, Emiliano Core, Alberto Narbona, and Carlos Selgasg. 2014. "Innovative passive and active countermeasures for near side crash safety. International Journal of Crashworthiness. 19(3): 209-221.

[2] C. R. Long, S., Chung Kim Yuena and G. N. Nuricka. 2019. Analysis of a car door subjected to side pole impact. Latin American Journal of Solids and Structures. 16(8): e226.

[3] Zhang G., Yu, F., OuYang Z. and Chen, H. 2015. Study on Vehicle Collision Predicting using Vehicle Acceleration and Angular Velocity of Brake Pedal. SAE Technical Paper 2015-01-1405.

[4] M. A. Shaharuzaman, S. M. Sapuan, M. R. Mansor and M. Y. M. Zuhri. 2018. Passenger car's side door impact beam: A review. Journal of Engineering and Technology. 9(1):.

[5] Yang J.-H. 2011. Optimization of the aluminum door impact beam considering the side door strength and the side impact capability. Journal of the Korea Academia Industrial Cooperation Society. 12(5):2025-2030.

[6] B. Watson and D.S. Cronin. 2011. Side impact occupant response with varying positions. International Journal of Crashworthiness. 16(5): 569-582.

[7] Haksung Lee, Mongyoung Huh, Shinjae Kang and Seok Il Yun. 2017. Design optimization of thin-walled circular tubular structures with graded thickness under later impact loading. International Journal of Automotive Technology. 18(3): 439-449.

[8] W. Abramowicz. 1981. Simplified crushing analysis of thin-walled columns and beams. Rozpr. Inzynierskie. 29(1): 5-26.

[9] Dušan Kecman. 1983. Bending collapse of rectangular and square section tubes. Int. J. Mech. Sci. 25(9): 623-636.

[10] Hamidreza Saadatfard, Abbas Niknejad, Gholamhossein Liaghat and Shahabeddin Hatami. 2019. A novel general theory for bending and plastic hinge line phenomena in indentation and flattening processes. Thin-Walled Structures. 136, 150-161.

[11] M. Elchalakani, X.L. Zhao and R.H. Grzebieta. 2002. Plastic mechanism analysis of circular tubes under pure bending. International Journal of Mechanical Sciences. 44 1117-1143.

[12] M. Kotelko, T.H. Lim, and J. Rhodes. 2002. Post-failure behaviour of box section beams under pure bending (an experimental study). Thin-Walled Structures. 38(2).

[13] Soheila Maduliat, Tuan Duc Ngo, Phuong Tran and Raymond Lumantarna. 2015. Performance of hollow steel tube bollards under quasi-static and lateral impact load. Thin-Walled Structures. 88, 41-47.

[14] S. Poonaya, U. Teeboonma and C. Thinvongpituk. 2009. Plastic collapse analysis of thin-walled circular tubes subjected to bending. Thin-Walled Structures. 47(6): 637-645.

[15] Haksung Lee, Mongyoung Huh, Shinjae Kang and Seok Il Yun. 2017. Compressive behavior of automotive side impact beam with continuous glass fiber reinforced thermoplastics incorporating long fiber thermoplastics ribs. Fibers and Polymers. 18(8): 1609-1613.

[16] Sof M. I., M, Chow Z. P., Wong K. J. and Ahmad Z. 2020. Study of multi-cell thin-walled tube with various configuration under lateral loading. Materials Science and Engineering. 884(1): 012086.

[17] Guangyao Li, Fengxiang Xu, Guangyong Sun and Qing Li. 2015. Crashworthiness study on functionally graded thin walled structures. International Journal of Crashworthiness,doi.org/10.1080/13588265.2015.1010396

[18] Sanjay D. Patil, Dheeraj S. Lengare, Arvind J. Bhosale, Kiran B. Bansode, and Rashtrapal B. Teltumade. 2020. Parameters affecting the specific energy absorption of circular side impact beam. International Journal of Engineering and Advanced Technology. 9(3).

[19] David Bilston, Dong Ruan, Artur Candidoand Yvonne Durandet. 2019. Parametric study of the cross-section

shape of aluminium tubes in dynamic three-point bending. Thin-Walled Structures. 136: 315-322.

[20] Zonghua Zhang, Shutian Liu and Zhiliang Tang. 2019. Design optimization of cross-sectional configuration of rib-reinforced thin-walled beam. Thin-Walled Structures. 47: 868-878.

[21] Ali Ghadianlou and Shahrir Bin Abdullah. 2013. Crashworthiness design of vehicle side door beams under low-speed pole side impacts. Thin-Walled Structures. 67, 25-33.

[22] Tao Tang, Weigang Zhang, Hanfeng Yin and Han Wang. 2016. Crushing analysis of thin-walled beams with various section geometries under lateral impact. Thin-Walled Structures. 102, 43-57.

[23] Xiong Zhang, Hui Zhang, Hui Zhang. 2016. Bending collapse of square tubes with variable thickness. International Journal of Mechanical Sciences. 106: 107-116.

[24] Amit Pathak, Anish Kumar and Rahul Lamba. 2017. Effect of beam layout and specification on side door strength of passenger cars: an experimental approach to analyze its effect and contribution to door strength. SAE Technical Paper 26-0023.

[25] F. Tarlochan A. N, F. Samer B, A.M.S. Hamouda C, S. Ramesh D and Karam Khalid. 2013. Design of thin wall structures for energy absorption applications: Enhancement of crashworthiness due to axial and oblique impact forces. Thin-Walled Structures. 71, 7-17.

[26] Hakim S. Sultan Aljibori, Haidar F. Al-Qrimli, Rahizar Ramli, E. Mahdi Faris Tarlochan and Chong W. P. 2018. A comparative Analysis of Experimental and Numerical Investigations of Composite, Tubes under Axial and Lateral Loading. Australian Journal of Basic and Applied Sciences, 4(8): 3077-3085.

[27] Muhammed Emin Erdin, Cengiz Baykasoglu and Merve Tunay Cetin. 2016. Quasi-static axial crushing behavior of thin-walled circular aluminum tubes with functionally graded thickness. Procedia Engineering. 149: 559-565.

[28] D.H. Chen, K. Masuda. 2016. Rectangular hollow section in bending: Part I - Cross-sectional flattening deformation. Thin-Walled Structures. 106: 495–507

[29] Patil S., Bhosale A., Dhepe V., Lengare D. & Kakde R. 2021. Impact Energy Absorption Capability of Polygonal Cross-Section Thin-Walled Beams under Lateral Impact. International Journal of Innovative Research and Scientific Studies, 4(4): 205-214. https://doi.org/10.53894/ijirss.v4i4.96